Journal of Hazardous Materials, 34 (1993) 173–197
Elsevier Science Publishers B.V., Amsterdam

Review

Computer modelling of turbulent gas explosions in complex 2D and 3D geometries

Bjørn H. Hjertager

Telemark Institute of Technology (TMIH) and Telemark Technological R & D Centre (TEL-TEK), Kjølnes, N-3900 Porsgrunn (Norway)

(Received March 3, 1992; accepted August 10, 1992)

Abstract

Numerical simulation methods capable of predicting flame and pressure development in turbulent gas explosions are presented. Special attention is given to methods which adopt the $k-\varepsilon$ model of turbulence. Several verification calculations are presented, which include a variety of geometrical layouts as well as a range of different fuel–air mixtures. Comparisons between simulated and measured explosion data are in general in good agreement.

1. Introduction

1.1 The problem

Gas explosion hazard assessment in flammable gas handling operations is crucial in obtaining an acceptable level of safety. In order to perform such assessments, good predictive tools are needed. These tools should take account of relevant parameters, such as geometrical design variables and gas cloud distribution. A theoretical model must therefore be tested against sufficient experimental data prior to becoming a useful tool. The experimental data should include variations in geometry as well as gas cloud composition and the model should give reasonable predictions without use of geometry or case-dependent constants.

1.2 Relevant works

It has in the past been usual to predict the flame and pressure development in vented volumes or unconfined vapour clouds by modelling the burning velocity of the propagating flame. This may be successful if we have a simple mode of flame propagation such as axial, cylindrical or spherical propagation in volumes *without obstructions* in the flow. If these are present, however, it is almost impossible to track the flame front throughout complex geometries. It has been

0304-3894/93/$06.00

apparent that in these situations it is more useful to model the propagation by calculating the rate of fuel combustion at different positions in the flammable volume. It is also important to have a model which is able to model both subsonic and supersonic flame propagation to enable a true prediction of what can happen in an accident scenario. One such model, which in principle meets all these needs, has been proposed by Hjertager and coworkers [1–5] and Bakke and Hjertager [6–8]. The model has been tested against experimental data from various homogeneous stoichiometric fuel–air mixtures in both large- and small-scale geometries. Similar models for gas explosions have subsequently also been proposed by Kjäldman and Huhtanen [9], Marx et al. [10], Martin [11] and Van den Berg [12]. All the above models are similar in nature. They use finite-domain approximations to the governing equations. Turbulence influences are taken account of by the $k-\varepsilon$ model of Launder and Spalding [13] and the rate of combustion is modelled by variants of the 'eddy dissipation' model of Magnussen and Hjertager [14]. The Bakke and Hjertager models are incorporated in two computer codes named FLACS (FLame Acceleration Simulator) and EXSIM (EXplosion SIMulator). The solution method used is the SIMPLE technique of Patankar and Spalding [15]. The model of Kjäldman and Huhtanen uses the general PHOENICS code of Spalding [16]. Whereas the model of Marx et al. uses the CONCHAS–SPRAY computer code which embodies the ICE–ALE solution technique [17]. The model of Van den Berg is similar to the Hjertager model and is incorporated into a code named REAGAS. Finally, the model of Martin which is embodied in a computer code named FLARE uses the flux-corrected transport (FCT) of Boris and Book [18].

1.3 Objectives

This paper will review the EXSIM simulation model, show some validation calculations and present some predicted scaling characteristics.

2. Governing equations

2.1 Mass and momentum

The problem of turbulent explosion can be handled by solving for the time-mean evolution of time-mean values of the dependent variables in the domain of interest. The time-mean of a variable varying with time, t, may be expressed as:

$$\Phi(t)=\frac{1}{T}\int_{t}^{t+T}\varphi(\tau)\,\mathrm{d}\tau \tag{1}$$

where $\Phi(t)$ is the time-mean of the instantaneous value $\varphi(t)$ averaged over the time interval T. T must satisfy two competing demands. First, it must be small enough not to smear out the sought time dependence of the system under consideration. Secondly, it must be large enough to be able to produce

sufficient information to enable relevant time-mean values in the interval. This means that time-mean values of both the relevant variables and their second order correlations must be obtainable in the time interval T. This is often possible since conversely, turbulence has higher frequencies than the large-scale motion which generates turbulence. The equations of motion and the energy equation can thus be expressed in tensor notation as:

$$\frac{\partial}{\partial t}\rho + \frac{\partial}{\partial x_j}(\rho U_j) = 0 \tag{2}$$

$$\frac{\partial}{\partial t}(\rho U_i) + \frac{\partial}{\partial x_j}(\rho U_j U_i) = -\frac{\partial p}{\partial x_i} + \frac{\partial}{\partial x_j}(\sigma_{ij}) + \rho g_i \tag{3}$$

$$\frac{\partial}{\partial t}(\rho h) + \frac{\partial}{\partial x_j}(\rho U_j h) = -\frac{\partial}{\partial x_j}(J_{h,j}) + \frac{\mathrm{D}p}{\mathrm{D}t} + S_h \tag{4}$$

Here $\partial\cdot/\partial t$ is the partial derivative, $\mathrm{D}\cdot/\mathrm{D}t$ the substantial derivative, U_j is the velocity component in the x_j coordinate direction; p is the pressure, ρ is the density; h is the enthalpy; σ_{ij} and $J_{h,j}$ are the turbulent fluxes of momentum and energy; g_i is the gravitational acceleration in the x_i-direction and S_h is the additional source term for enthalpy.

2.2 Chemical species

The combustion is treated as a single-step irreversible chemical reaction with finite reaction rate between fuel and oxygen. Hence, the reaction scheme may be written as:

$$1\,\text{kg fuel} + s\,\text{kg oxygen} \longrightarrow (1+s)\,\text{kg products} \tag{5}$$

Here s is the stoichiometric oxygen requirement to burn 1 kg of fuel. This simple reaction scheme results in the mixture composition being determined by solving for only two variables, namely, mass fraction of fuel, Y_{fu}, and the mixture fraction, f.

$$\frac{\partial}{\partial t}(\rho Y_{\mathrm{fu}}) + \frac{\partial}{\partial x_j}(\rho U_j Y_{\mathrm{fu}}) = -\frac{\partial}{\partial x_j}(J_{\mathrm{fu},j}) + R_{\mathrm{fu}} \tag{6}$$

$$\frac{\partial}{\partial t}(\rho f) + \frac{\partial}{\partial x_j}(\rho U_j f) = -\frac{\partial}{\partial x_j}(J_f) \tag{7}$$

Here R_{fu} is the time-mean rate of combustion of fuel, whereas $J_{\mathrm{fu},j}$ and $J_{f,j}$ are the diffusive fluxes in the x_j-direction. The basis for this to be valid is that the Schmidt numbers are equal for all species, an approximation which is often found in turbulent flows.

The mixture fraction is defined as:

$$f = \frac{\xi - \xi_\infty}{\xi_0 - \xi_\infty} \tag{8}$$

where ξ is a conserved combined variable of, for example, mass fraction of fuel, Y_{fu} and mass fraction of oxygen, Y_{O_2}, expressed as:

$$\xi = Y_{fu} - \frac{Y_{O_2}}{s} \tag{9}$$

ξ_0 is the value of ξ at a fuel-rich reference point, for example, a fuel leakage point in the domain, and ξ_∞ is the value of ξ at an oxygen-rich reference point, for example, the ambient air condition. For a homogeneous premixed system the mixture fraction will be constant in the domain of interest and consequently only the Y_{fu} equation needs to be solved.

3. Turbulence and combustion models

3.1 General

To solve the governing equations (2), (3), (4), (6) and (7) given above the fluxes, σ_{ij} and $J_{\Phi,j}$, and the rate of combustion, R_{fu}, have to be modelled together with specification of relevant boundary conditions. Both the fluxes and the combustion rate are time-mean averaged values of fluctuating quantities. The fluxes can, for a general variable, Φ, and a velocity component U_j, be expressed as:

$$J_{\Phi,j} = -\overline{\rho u_j \varphi} \tag{10}$$

and

$$\sigma_{ij} = -\overline{\rho u_i u_j} \tag{11}$$

where u_i and φ are the instantaneous fluctuations around the time-mean values U_i and Φ, respectively. The overbar indicates time-mean value over the time interval T as defined in expression (1). When modelling the correlations given in (10) and (11) it is usual to relate these to the product of time-mean gradients of the relevant variables and an effective turbulent transport coefficient. For a general scalar variable Φ and a velocity component U_j the relations are:

$$J_{\Phi,j} = -\frac{\mu_{eff}}{\sigma_\Phi}\frac{\partial \varphi}{\partial x_j} \tag{12}$$

and

$$\sigma_{ij} = \mu_{eff}\left(\frac{\partial U_i}{\partial x_j} + \frac{\partial U_j}{\partial x_i}\right) - \frac{2}{3}\delta_{ij}\left(\rho k + \mu_{eff}\frac{\partial U_k}{\partial x_k}\right) \tag{13}$$

respectively.

Here $\delta_{ij} = 1$ if $i = j$ and $\delta_{ij} = 0$ if $i \neq j$. An effective viscosity μ_{eff} and the kinetic energy of turbulence have been introduced in the above expressions, together with an effective Prandtl/Schmidt number σ_Φ. The kinetic energy of turbulence, k, is related to the fluctuating turbulence velocity components in the

three coordinate directions as:

$$k = \tfrac{1}{2}(\overline{u_1^2} + \overline{u_2^2} + \overline{u_3^2}) \tag{14}$$

The effective turbulence viscosity is given by two turbulence parameters, the isotropic turbulence velocity u_t and a length scale, l as:

$$\mu_{\text{eff}} = \mu_l + \rho u_t l \tag{15}$$

μ_l is the molecular viscosity. The determination of the turbulence velocity and length scale are done by use of a turbulence model.

3.2 Two-parameter turbulence model

The determination of u_t and l are done by application of the so-called $k-\varepsilon$ model of turbulence given by Launder and Spalding [13]. The turbulence velocity is related to the kinetic energy of turbulence, k, as:

$$u_t = \sqrt{\frac{2}{3}k} \tag{16}$$

and the length scale, l, is related to the kinetic energy of turbulence, k, and its rate of dissipation ε, as:

$$l \sim \frac{k^{3/2}}{\varepsilon} \tag{17}$$

Inserting eqs. (16) and (17) into expression (15) gives as the result:

$$\mu_{\text{eff}} = \mu_l + C_\mu \rho \frac{k^2}{\varepsilon} \tag{18}$$

C_μ is a constant taken to be 0.09 (Launder and Spalding [13]). The conservation equations that determine the distribution of k and ε read as:

$$\frac{\partial}{\partial t}(\rho k) + \frac{\partial}{\partial x_j}(\rho U_j k) = \frac{\partial}{\partial x_j}\left(\frac{\mu_{\text{eff}}}{\sigma_k}\frac{\partial k}{\partial x_j}\right) + G - \rho\varepsilon \tag{19}$$

$$\frac{\partial}{\partial t}(\rho \varepsilon) + \frac{\partial}{\partial x_j}(\rho U_j \varepsilon) = \frac{\partial}{\partial x_j}\left(\frac{\mu_{\text{eff}}}{\sigma_\varepsilon}\frac{\partial \varepsilon}{\partial x_j}\right) + C_1\frac{\varepsilon}{k}G - C_2\rho\frac{\varepsilon^2}{k} \tag{20}$$

The two new constants appearing above C_1 and C_2, are given the values 1.44 and 1.79 respectively. The Schmidt numbers σ_k and σ_ε are given the values 1.0 and 1.3, respectively, whereas the other Schmidt/Prandtl numbers are put equal to 0.7. The generation rate of turbulence is given by:

$$G = \sigma_{ij}\frac{\partial U_j}{\partial x_i} \tag{21}$$

These production terms take account of turbulence produced by shear and compression/expansion. If buoyancy production or Rayleigh–Taylor instability production is important additional terms may be added.

3.3 Rate of combustion

The rate of combustion may be modelled according to the 'eddy-dissipation' concept by Magnussen and Hjertager [14] with the ignition/extinction modification introduced by Hjertager [2] and the quasi-laminar combustion modification introduced by Bakke and Hjertager [6].

If the local turbulent Reynolds number, based on the turbulent velocity and length scale, is less than a critical value the rate of combustion is calculated according to:

$$R_{fu} = -A_{lam} n_t \frac{S_{lam}}{\delta_f} \rho Y_{lim} \tag{22}$$

Here n_t is the enhancement factor related to the wrinkling of the laminar flame and this factor is proportional to the radius of flame propagation up to a maximum radius of 0.5 m. The enhancement factor is 1.0 for a radius of 0 m and is 2.5 for radii larger than 0.5 m. S_{lam} and δ_f are the laminar burning velocity and thickness of the laminar flame, A_{lam} is a constant.

If the local turbulent Reynolds number is larger than the critical value, the rate of combustion is calculated according to the eddy dissipation approach modified by the extinction/ignition criteria.

Two time scales are defined, namely, the turbulent eddy mixing time scale, $\tau_e = k/\varepsilon$, and the chemical time scale:

$$\tau_{ch} = A_{ch} \exp\left(\frac{E}{RT}\right) (\rho Y_{fu})^a (\rho Y_{O_2})^b \tag{23}$$

Also, an ignition/extinction criterion is defined when the two time scales are in a certain ratio $(\tau_{ch}/\tau_e)^* = D_{ie}$. The rate of combustion is thus calculated as:

$$\begin{aligned} R_{fu} &= 0 \quad \text{when} \quad \frac{\tau_{ch}}{\tau_e} > D_{ie} \\ R_{fu} &= -\frac{A}{\tau_e} \rho Y_{lim} \quad \text{when} \quad \frac{\tau_{ch}}{\tau_e} < D_{ie} \end{aligned} \tag{24}$$

where Y_{lim} is the smallest of three mass fractions, namely, fuel, Y_{fu}, oxygen Y_{O_2}/s, or mass fraction of fuel already burnt, $Y_{fu,b}$, A and D_{ie} are two constants.

4. Modelling of complex geometries

Many geometries found in industrial practice may contain a lot of geometrical details which can influence the process to be simulated. Examples of such geometries are heat exchangers with thousands of tubes and several baffles, and regenerators with a lot of internal heat absorbing obstructions, etc. In the present context, the geometries found inside modules on offshore oil and gas-producing platforms and geometries found in refineries constitute relevant examples of the complex geometries at hand. There are at least two routes for

describing such geometries. First, we may choose to model every detail by use of very fine geometrical resolution, or secondly, we may describe the geometry by use of some suitable bulk parameters. Detailed description will always need large computer resources both with regard to memory and calculation speed. It is not feasible with present or even with future computers to implement the detailed method for solving such complex problems. We are therefore forced to use the second line of approach, which incorporates the porosity/distributed resistance formulation of the governing equations. This method was proposed by Patankar and Spalding [19] and has been applied to analysis of heat exchangers, regenerators and nuclear reactors. Sha et al. [20] have extended the method to include advanced turbulence modelling.

The presence of geometrical details modifies the governing equations in two ways. First, only part of the total volume is available to flow and secondly solid objects offer additional resistance to flow and additional mixing in the flow. The modified equations for use in high density geometries may be expressed by:

$$\frac{\partial}{\partial t}(\beta_v \rho\phi)+\frac{\partial}{\partial x_i}(\beta_i \rho U_i \phi)=\frac{\partial}{\partial x_i}\left[\beta_i \Gamma \frac{\partial \phi}{\partial x_i}\right]+\beta_v(S_\phi+R_\phi) \tag{25}$$

Here ϕ denotes a general variable. β_v is the volume fraction occupied by the fluid, β_i is the area fraction available for flow in the x_i-direction and R_ϕ is the additional resistance or additional mixing or heat transfer caused by solid obstructions in the flow. All the volume/area fractions (porosities) may take values between 0.0, completely blocked, or 1.0, completely open. Some R_ϕ functions may be found in a report by Sha and Launder [21]. These functions depend on parameters like velocity, porosity, typical dimension, pitch between obstacles, obstacle shape and orientation.

5. Solution procedures

It is noted that all conservation equations mentioned above can be written in the following general form (all porosities are set equal to unity for clarity):

$$\frac{\partial}{\partial t}(\rho\Phi)+\frac{\partial}{\partial x_j}(\rho U_j \Phi)=\frac{\partial}{\partial x_j}\left(\Gamma_\Phi \frac{\partial \Phi}{\partial x_j}\right)+S_\Phi; \qquad \Gamma_\Phi=\frac{\mu_{\text{eff}}}{\sigma_\Phi} \tag{26}$$

I II III IV

This means, equations with four distinct terms, namely, I transient, II convection, III diffusion and IV source terms. A summary of all the equations needed for a typical calculation of flows with chemical reaction is given in Table 1. Solution of these equations are performed by finite-domain methods. Details of the computation methods are given by Hjertager [1] and Bakke and Hjertager [7]. Only a brief description of the solution method adopted by Hjertager [1, 2] is given here.

TABLE 1

Conservation equations

Conservation of	Φ	σ_Φ	S_Φ
Mass	1.0	∞	0
Velocity in x-direction	U	1.0	$-\frac{\partial p}{\partial x}+\frac{\partial}{\partial x}\left(\mu_{\text{eff}}\frac{\partial U}{\partial x}\right)+\frac{\partial}{\partial y}\left(\mu_{\text{eff}}\frac{\partial V}{\partial x}\right)+\frac{\partial}{\partial z}\left(\mu_{\text{eff}}\frac{\partial W}{\partial x}\right)-\frac{2}{3}\frac{\partial}{\partial x}\left(\mu_{\text{eff}}\cdot\nabla\cdot U+\rho k\right)$
Velocity in y-direction	V	1.0	$-\frac{\partial p}{\partial y}+\frac{\partial}{\partial x}\left(\mu_{\text{eff}}\frac{\partial U}{\partial y}\right)+\frac{\partial}{\partial y}\left(\mu_{\text{eff}}\frac{\partial V}{\partial y}\right)+\frac{\partial}{\partial z}\left(\mu_{\text{eff}}\frac{\partial W}{\partial y}\right)-\frac{2}{3}\frac{\partial}{\partial y}\left(\mu_{\text{eff}}\cdot\nabla\cdot U+\rho k\right)$
Velocity in z-direction	W	1.0	$-\frac{\partial p}{\partial z}+\frac{\partial}{\partial x}\left(\mu_{\text{eff}}\frac{\partial U}{\partial z}\right)+\frac{\partial}{\partial y}\left(\mu_{\text{eff}}\frac{\partial V}{\partial z}\right)+\frac{\partial}{\partial z}\left(\mu_{\text{eff}}\frac{\partial W}{\partial z}\right)-\frac{2}{3}\frac{\partial}{\partial z}\left(\mu_{\text{eff}}\cdot\nabla\cdot U+\rho k\right)$
Kinetic energy of turbulence	k	σ_k	$G-\rho\varepsilon$
Rate of dissipation	ε	σ_ε	$\frac{\varepsilon}{k}(C_1G-C_2\varepsilon)$
Enthalpy	h	σ_h	$\frac{\partial p}{\partial t}+U\frac{\partial p}{\partial x}+V\frac{\partial p}{\partial y}+W\frac{\partial p}{\partial z}$
Mass fraction of fuel	Y_{fu}	σ_{fu}	R_{fu}
Mixture fraction	f	σ_f	0

$$G=\mu_{\text{eff}}\left\{2\left[\left(\frac{\partial U}{\partial x}\right)^2+\left(\frac{\partial V}{\partial y}\right)^2+\left(\frac{\partial W}{\partial z}\right)^2\right]+\left(\frac{\partial U}{\partial y}+\frac{\partial V}{\partial x}\right)^2+\left(\frac{\partial U}{\partial z}+\frac{\partial W}{\partial x}\right)^2+\left(\frac{\partial W}{\partial y}+\frac{\partial V}{\partial z}\right)^2\right\}-\frac{2}{3}\nabla\cdot\vec{U}(\mu_{\text{eff}}\cdot\nabla\cdot U+\rho k)$$

$$\nabla\cdot U\equiv\frac{\partial U}{\partial x}+\frac{\partial V}{\partial y}+\frac{\partial W}{\partial z}$$

The calculation domain is divided into a finite number of main grid points where pressure p, density ρ, mass fraction of fuel, Y_{fu}, mixture fraction f, and the two turbulence quantities k and ε are stored. The three velocity components U, V and W are, on the other hand, stored at grid points located midway between the main points. The conservation equations are integrated over control volumes surrounding the relevant grid points in space, and over a time interval, Δt. This integration is performed using upwind differencing and implicit formulation.

The result of this is a set of non-linear algebraic equations, which are solved by application of the well known tri-diagonal matrix algorithm used along the three coordinate directions. Special care has been taken to solve the pressure/velocity/density coupling of the three momentum equations and the mass balance. The 'SIMPLE' method developed by Patankar and Spalding [15] for three-dimensional incompressible parabolic flow has been extended by Hjertager [1] to compressible flows and is used to handle this coupling. The method introduces a new variable, the so-called pressure correction which makes the necessary corrections to the velocity components, pressure and density to make them obey the mass balance constraint at the new time level. The pressure correction is determined by solution of a set of algebraic equations derived from the linearized momentum equations and the mass balance equation.

6. Validation calculations

6.1 Tube

Calculations of flame and pressure development have been performed for three different homogeneous fuel–air mixtures contained in two different tube geometries. The methane–air and propane–air data [22–24] used are taken from a large-scale explosion study in a 50 m^3 tube of 2.5 m diameter and 10 m length with five orifice rings of variable blockage ratios.

The hydrogen/air data used are taken from a small-scale experimental study performed by Lee et al. [25]. This geometry was a tube, 5 cm in diameter and 3 m in length, having orifice rings which blocked off 60% of the free tube area and with distance between rings of 5 cm. These tests comprise a fairly large span in both scale and fuel type and are thus suited for our present validation needs.

The chemical times are taken from Burcat et al. [26] and Schott and Kinsey [27], and the relevant parameters used in expression (23) are compiled in Table 2.

Figure 1 shows a comparison between experiments and predictions of peak pressures versus blockage ratio ($BR = 1 - (d/D)^2$) for methane–air and propane–air mixtures. The figure shows that the large difference in peak pressures between methane–air and propane–air explosions is fairly well predicted. The present prediction method also gives the correct behaviour of pressure versus blockage ratio. There is, however, some underprediction for propane–air at

TABLE 2

Fuel	A_{ch}	a	b	E/R (K^{-1})	Reference
Methane	3.62×10^{-14}	0.33	−1.03	23.300	Burcat et al. [26]
Propane	4.40×10^{-14}	0.57	−1.22	21.210	Burcat et al. [26]
Hydrogen	2.25×10^{-11}	0	−1.0	9.132	Schott and Kinsey [27]

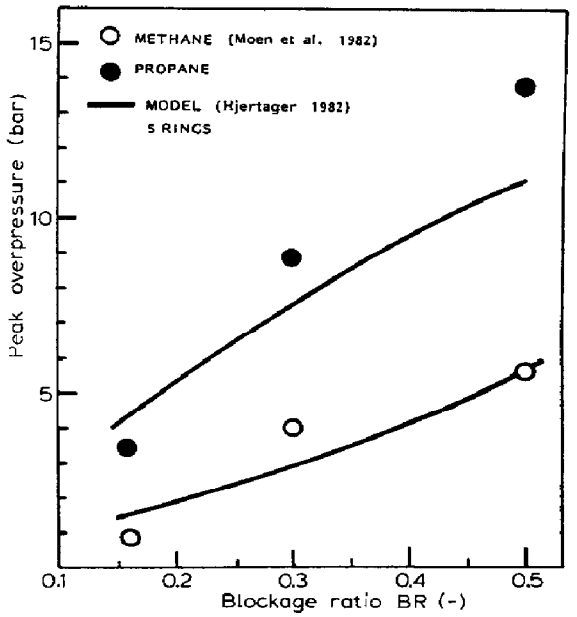

Fig. 1. Peak measured [22, 23] and predicted pressures in the 50 m^3 combustion tube as a function of blockage ratio, $BR = 1 - (d/D)^2$. Propane–air and methane–air mixtures.

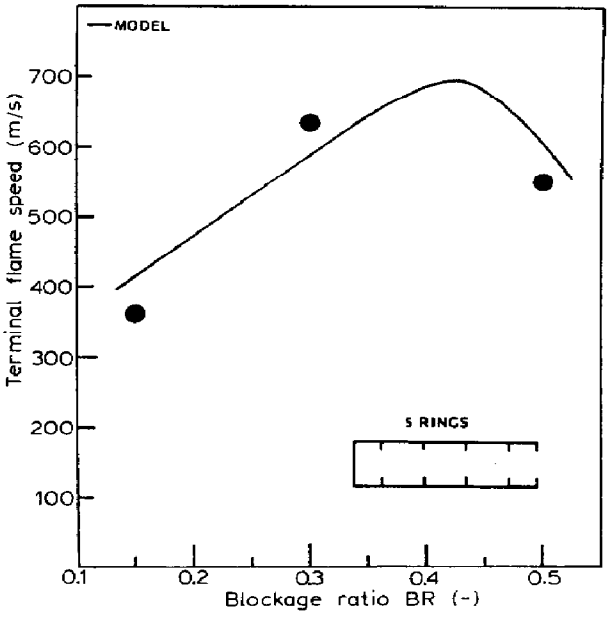

Fig. 2. Comparison between measured (Hjertager et al. [23]) and predicted variations of terminal flame speed with blockage ratio.

blockage ratio 0.5. It should also be mentioned that the original combustion rate model [1] would only show a 20% difference between methane and propane. This clearly demonstrates that only changes in thermodynamic properties and the infinite chemical kinetics assumption are incapable of reproducing the experimental differences between methane–air and propane–air explosions.

Figure 2 shows a comparison between the computation model and the experiments of the terminal flame speed for propane–air as a function of blockage ratio. It is seen that the agreement is satisfactory and that the

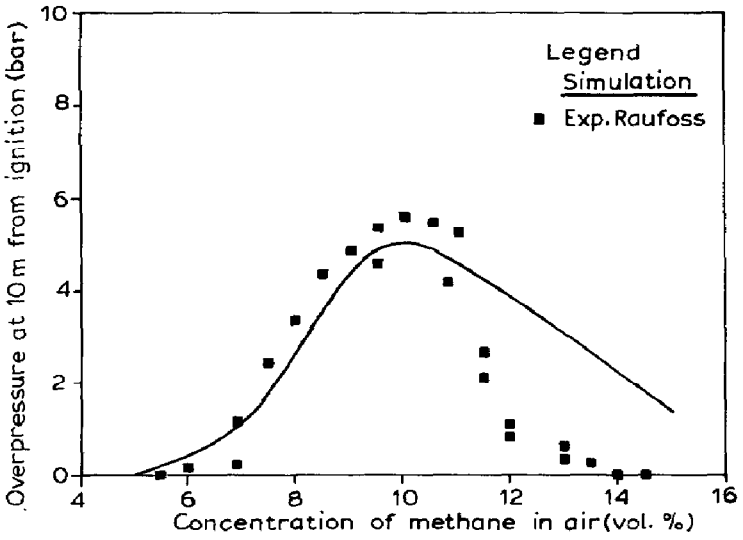

Fig. 3. Comparison of measured [24] and predicted peak overpressures at the exit of the 50 m^3 tube versus concentration of methane.

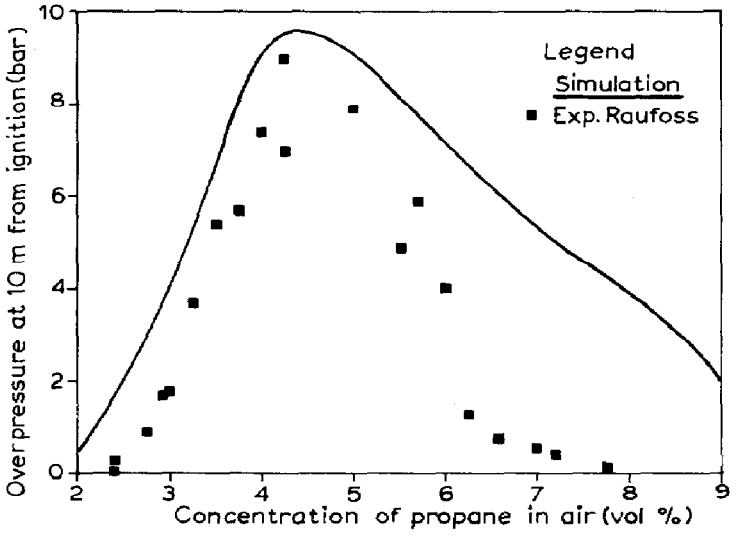

Fig. 4. Comparison of measured [24] and predicted peak overpressures at the exit of the 50 m^3 tube versus concentration of propane.

model predicts the optimum flame speed at a blockage ratio equal to approximately 0.4.

Figures 3 and 4 show a comparison between predicted and measured peak pressures for variable concentrations of methane–air and propane–air explosions in the 50 m^3 tube. Good agreement between predictions and

experiments can be observed for the lean mixtures of methane–air and propane–air, whereas less agreement is seen for both gases at the rich side of stoichiometry. There is a good correspondence between measured and predicted concentrations for optimum pressure build-up. Both mixtures exhibit this maximum at slightly rich mixtures. This is the same trend as found in detonation sensitivity studies in both methane–air and propane–air mixtures [28]. The predicted maximum peak pressures are approximately 5 bar for methane and 9.5 bar for propane. This difference has come about mainly because of different reaction times. Figures 5 and 6 elucidate this in more detail. These figures show local distributions within the tube of velocity, flame contours and reaction rate contours for both fuels. In Figs. 5(a) and (b) the conditions after the flame has passed the first obstacle are shown. We can see that the local distribution of all variables is almost identical for both gases. However, in Figs. 6(a) and (b), which show the situation after the flame has propagated over the second obstacle, some differences can be observed. At this position of the flame the turbulent mixing time, τ_e, has diminished to a value which corresponds to quenching in some regions where the shear in the flow is

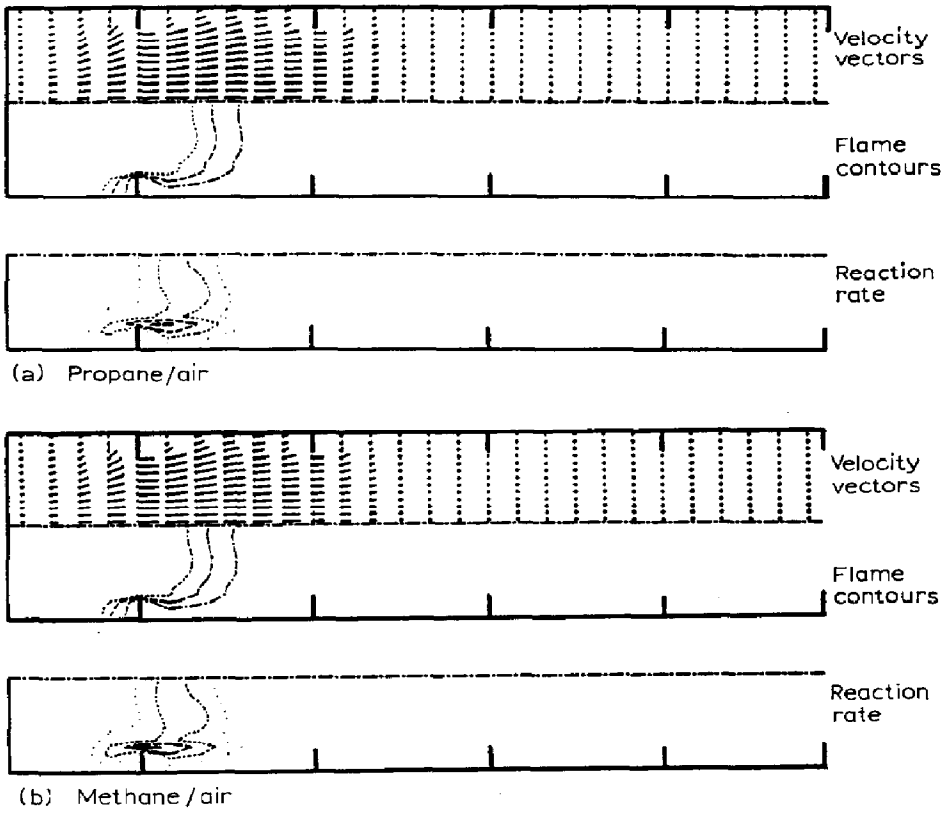

Fig. 5. Distribution of velocity, flame and reaction rate for (a) propane–air and (b) methane–air explosions after the flame has passed the first obstacle.

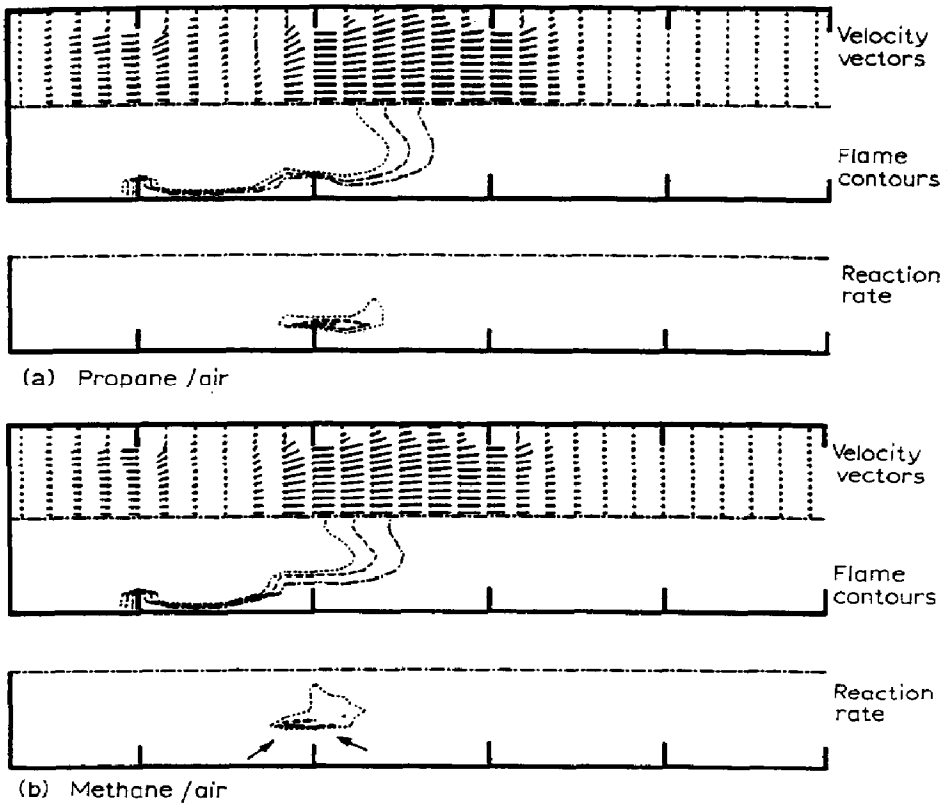

Fig. 6. Distribution of velocity, flame and reaction rate for (a) propane–air and (b) methane–air explosions after the flame has passed the second obstacle. Arrows indicate quenched regions.

large. Obviously, as seen in Fig. 6, this quenching is most pronounced for the methane–air mixture, since the chemical induction time is much larger for methane compared to propane. The arrows in Fig. 6(b), indicate the extinction region of the methane–air flame. This difference in flame propagation between methane and propane continues also for the rest of the flame travel. The net result of this is as shown in Figs. 3 and 4, that the pressures produced in methane–air explosions are lower by a factor of approximately 2 compared to propane–air explosions for identical geometries.

In Figs. 7 and 8 the comparisons between predictions and measurements are shown of flame speed and pressure produced in different hydrogen–air mixtures. It is seen that the agreement is in general good. The overall behaviour is well predicted for both quantities. However, if we look at the details, there are some discrepancies. These are especially notable close to stoichiometry where the experimental data show a sudden jump to a quasi-detonation. This is not seen in the corresponding predictions. Also, the experimentally observed jump in flame speed close to 13% hydrogen concentration is not well predicted. However, the predicted curve in Fig. 7 gives a good indication of the trend. As

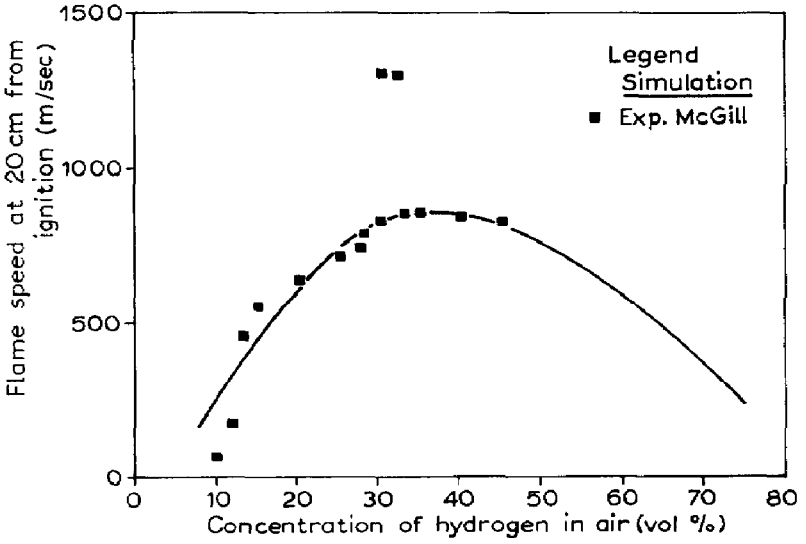

Fig. 7. Comparison of measured [25] and predicted flame speeds at 20 cm from ignition as a function of hydrogen concentration.

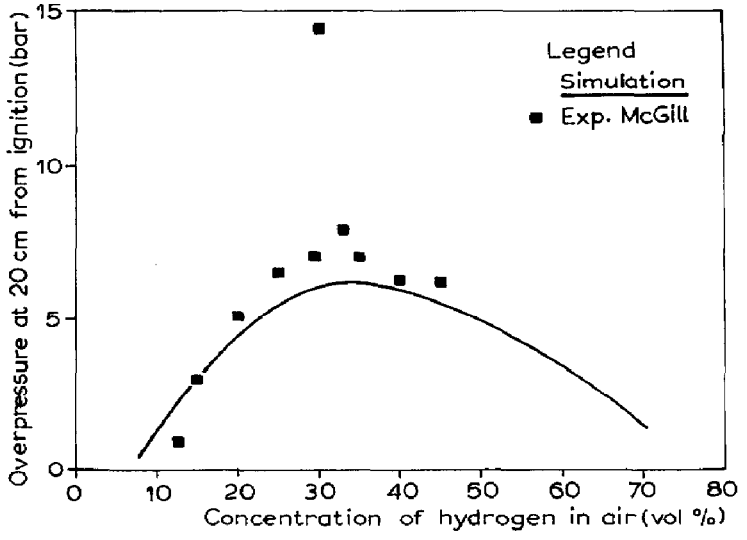

Fig. 8. Comparison of measured [25] and predicted peak overpressures at 20 cm from ignition as a function of hydrogen concentration.

noted by Lee et al. [25] the sudden jump in flame speed in Fig. 7 is probably due to a sudden change in reaction times. In order to model this correctly, a much more detailed reaction kinetic scheme than the simple induction time formula presently used, would be required.

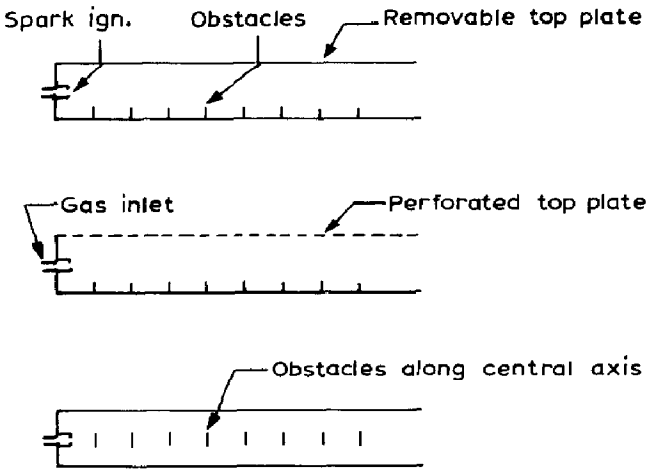

Fig. 9. Schematics of experimental apparatus (Chan et al. [29]).

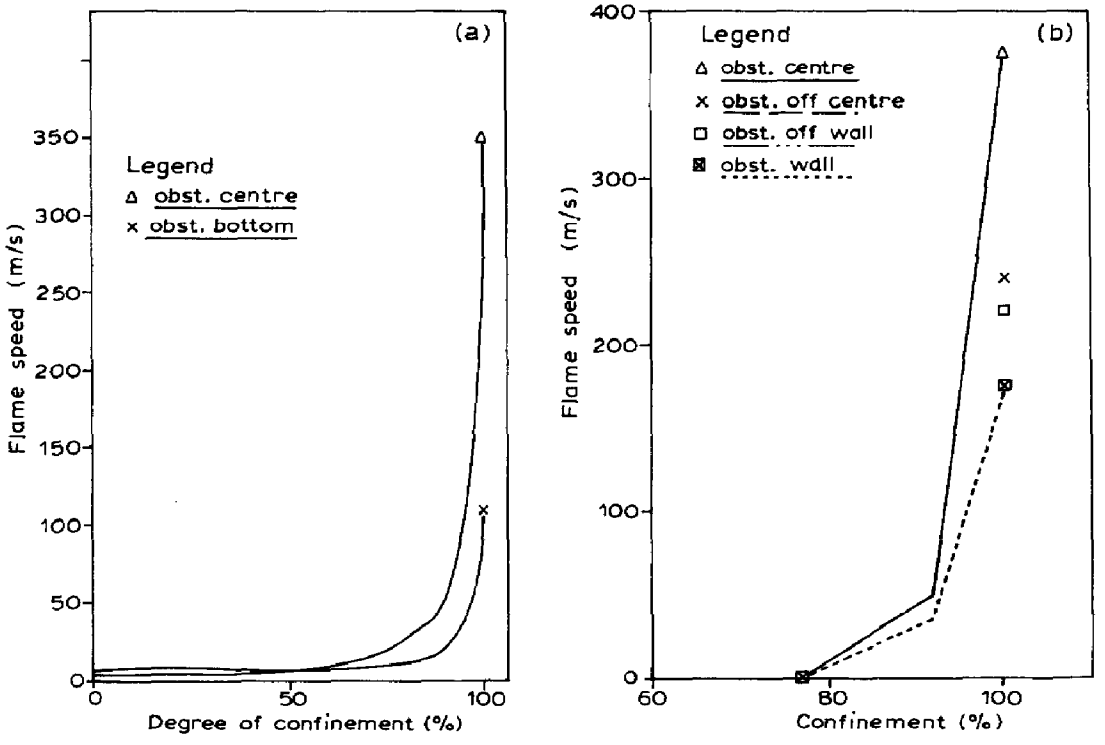

Fig. 10. (a) Measured flame speeds vs. confinement. Measured 1 m from ignition. (Chan et al. [29]). (b) Predicted flame speed vs. confinement. Calculated 1 m from ignition (Bakke and Hjertager [7]).

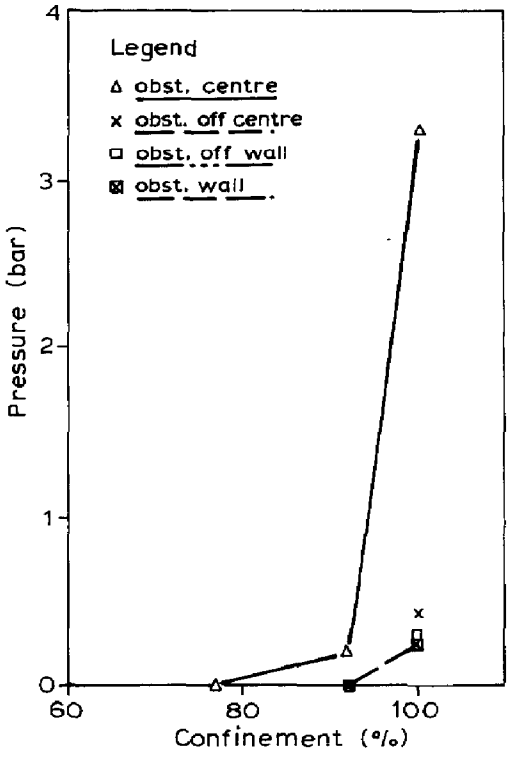

Fig. 11. Pressure vs. confinement. Monitored near lid and open end; maximum value (Bakke and Hjertager [7]).

6.2 Vented channel

As can be seen from the previous confinement on either side of the flame propagation path, high flame speeds and pressures are produced. Chan et al. [29] have performed a small scale study in which they investigated the influence of variable venting in a channel along the propagation path. The layout of their channel is shown in Fig. 9. The length of the channel was 1.22 m and the height was 0.203 m with sharp edged repeated obstacles which block off approximately 25% of the free channel area. The experiments were performed using a homogeneous stoichiometric mixture of methane in air. They found that the flame speed was drastically reduced by reducing the top confinement. This is shown in Fig. 10(a). Bakke and Hjertager [7] used these data in a validation study of the model presented above. Figure 10 shows a comparison between the measured and predicted variation of flame speed versus degree of confinement. The figure shows that there is close agreement between predictions and experiments. Both the decrease in flame speed and the difference between obstacles along the wall and along the centre line are fairly well reproduced. Also shown in Fig. 10 is the influence of moving the obstacles off the wall and off the centre line. Both of these cases show flame speeds in between the two extremes. Figure 11 shows the predicted peak pressures versus confinement. We observe

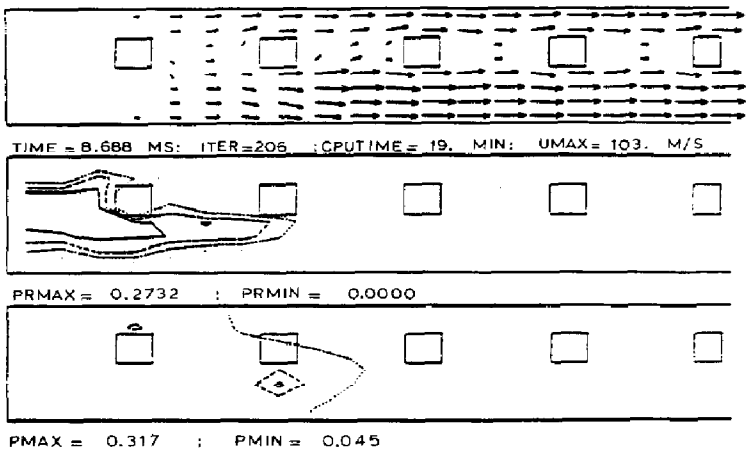

(a) Obstacles slightly off-centre line

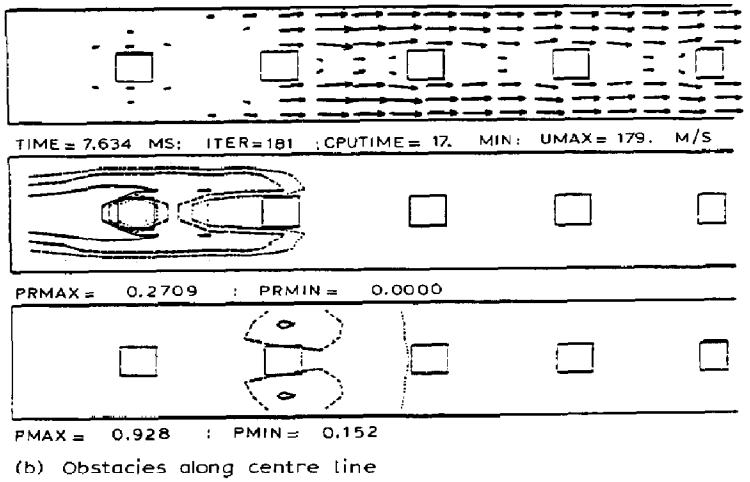

(b) Obstacles along centre line

Fig. 12. Distribution of velocity vectors, flame contours and pressure distribution for 100% confinement and two different obstacle arrangements (Bakke and Hjertager [7]): (a) obstacles slightly off centre line; (b) obstacles along centre line.

that the maximum pressure of over 3 bars is obtained by placing the obstacles along the centre line, whereas moving the obstacles towards the wall reduced the pressures by a factor of 10 in this particular geometry. This shows that the maximum effectiveness of two shear layers are only obtained when the obstacles are exactly in the centre line. Figure 12 shows the predicted distribution of flow velocities, flame contours and pressure contours for these two situations.

Moen et al. [30] have reported results from large-scale tests performed in a top-vented channel of 1.8 m × 1.8 m in cross section and 15.5 m in length with repeated obstacles. Results are given for three different stoichiometric fuel–air clouds, namely, acetylene, propane and hydrogen sulphide. Moen et al. [30]

TABLE 3

Fuel	A_{ch}	a	b	E/R	Reference
Acetylene	3.31×10^{-12}	0	−1.0	8.597	Kistiakowsky and Richards [31]
Hydrogen sulphide	5.0×10^{-13}	−0.45	−0.33	13.100	Frenklach et al. [32]

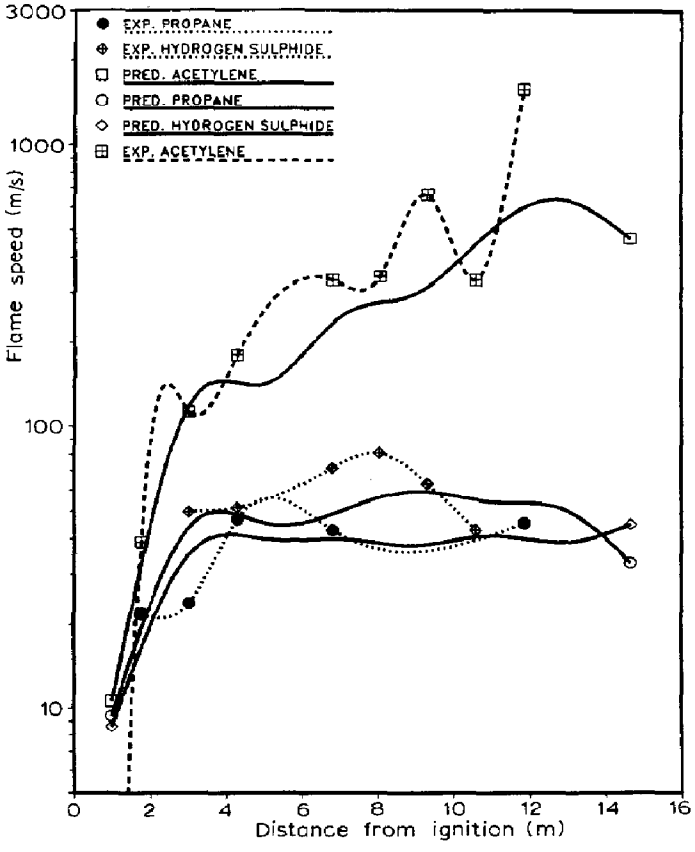

Fig. 13. Comparisons of measured and predicted (Moen et al. [30]) flame speeds along the 15.5 m vented channel.

also include results from application of the FLACS model to some of the experimental tests. The induction time data used in the calculations for acetylene and hydrogen sulphide are given in Table 3. Calculations are performed for one geometrical layout consisting of obstacles of diameter 0.5 m, pitch equals 1.25 m and a height above ground of 0.9 m.

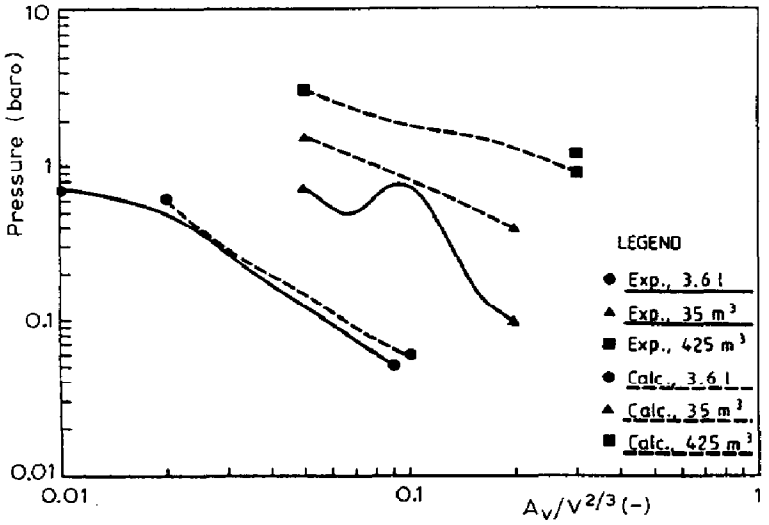

Fig. 14. Measured [33] and predicted (Bakke and Hjertager [8]) peak pressures as a function of the vent parameter for three different empty vessels.

Figure 13 shows comparisons between predicted and measured flame speeds along the 15.5 m length of the obstructed channel. The general characteristics of the observed differences between the three fuels seem to be well predicted. Propane and hydrogen sulphide explosions exhibits much lower flame acceleration compared to acetylene which accelerates to detonation at the end of the channel. The model is not able to predict this sudden transition to detonation due to the fact that only a turbulent combustion model is included.

6.3 Empty volumes

All the cases presented above contain internal obstructions inside the volume. Bakke and Hjertager [8] have applied the model to the empty volume propane–air tests of Solberg [33]. These tests included three different vessels without obstacles with volumes ranging from 3.6 l and up to 425 m^3.

Figure 14 shows a comparison between predicted and measured variation of the explosion pressure as a function of the scaled vent area. As we can see, the predictions are in reasonable agreement with measurements for all three volumes.

6.4 Module geometries

Hjertager et al. [4] have incorporated the model given above into a 3D computer code and used this to simulate the module data of Hjertager et al. [34]. The compressor module was modelled by using a grid of $42 \times 14 \times 14$ points in the length, height and width directions respectively. The internal equipment was modelled using approximately 100 obstructions. Figure 15 gives a summary of the simulated and measured peak pressure data in the 1:33 and 1:5 scale compressor modules. The figure shows a variation of

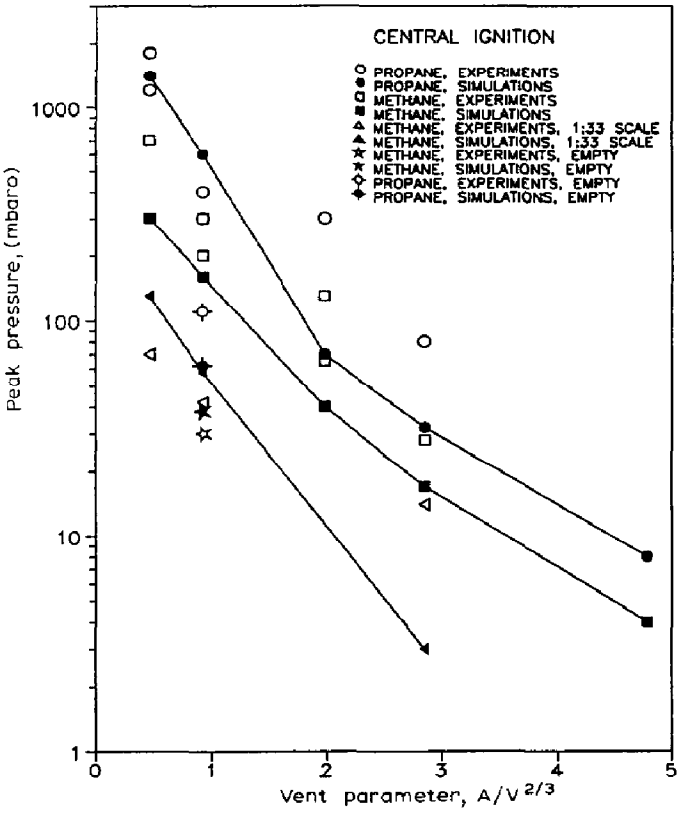

Fig. 15. Peak pressure as a function of vent parameter for centrally ignited explosions in the 1:5 scale compressor module – comparison between experiments and simulations. (Reproduced from [4] by permission of the publishers, Butterworth Heinemann Ltd. © 1992)

peak explosion pressures inside the module for centrally ignited clouds as a function of the vent parameter. It can be noted that the predicted general trends are in good accordance with the measurements. The computer model is able to predict the following characteristics found in the experiments:

1. The variation of peak pressures with the vent parameter.
2. The difference between pressure build-up in methane–air and propane–air explosions.
3. The influence of two scales, i.e. 1:33 and 1:5.
4. The influence of internal process equipment on the violence of the explosion.

Although the general trends are predicted well, it is also noted that there are discrepancies between experiments and simulations. This is especially seen for the cases with vent parameters larger than about 2.0 and for the 1:5 scale methane–air test with a vent parameter of about 0.5.

6.5 Scenario calculations

Hjertager et al. [5] have used the 3D gas explosion code to analyse the Piper Alpha accident. The geometrical and other data were taken from the interim

TABLE 4

Case	Peak pressure (bar)
1	4.7
2	0.68
3	0.86
4	0.15

report from the investigation of the Piper Alpha accident [35]. The explosion in the module C – the compression module – was modelled using a grid of $47 \times 17 \times 9$ points in the length, width and height directions. The internal equipment was modelled using about 55 obstructions.

Four different cases were simulated with a fixed ignition point located centrally in the module, namely stoichiometric homogeneous cloud filling:

1. the whole free space.
2. the right half of the free space.
3. the lower half of the free space.
4. one quarter of the free space located at the lower right position.

Table 4 gives the peak pressures that were found for the four cases: The table indicates a range of pressure loads from 150 mbar to 4.7 bar. The Piper Alpha report indicates that the pressures must have been larger than about 300 mbar. The model simulations indicate that three of the cases produce pressure loads larger than that. Even the case with one quarter of the module filled with flammable gas produces an explosion pressure that may produce significant damage.

Hjertager et al. [36] have demonstrated a scenario analysis of gas explosions on an onshore process plant. The results show that the explosion pressures for the four cases considered ranged from 0.2 bars and up to 9 bars. The highest pressure was found when ignition is in a partially confined area, thus producing an initially fast flame. The peak flame speeds range from approximately 200 m/s and up to 1200 m/s.

7. Scaling characteristics

This last section will report on some predicted scaling characteristics of fuel–air explosions contained in tubes with length over a diameter ratio $L/D = 4.0$ and with five orifice rings (obstacles) which block off 30% of the free tube area, and in channels with $L/D = 6.0$ and five obstacles which block off 25% of the free channel area. The obstacles are evenly distributed along the

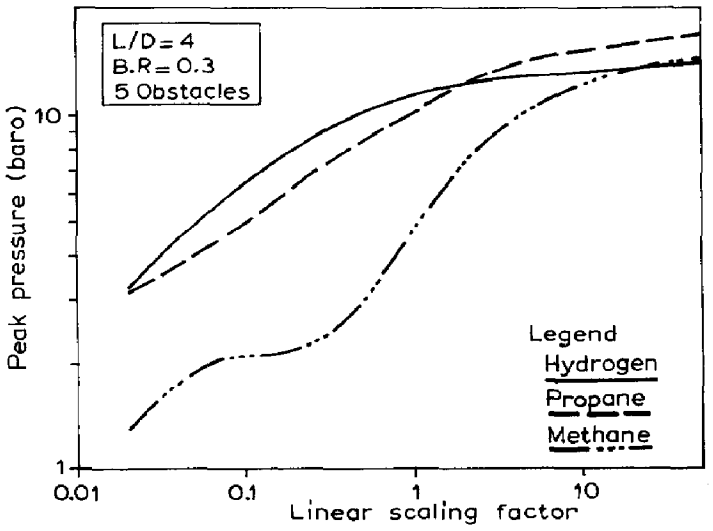

Fig. 16. Variation of peak overpressure in stoichiometric mixtures of methane–air, propane–air and hydrogen–air with scaling. Scaling factor of 1.0 indicates 10 m of flame travel over five obstacles.

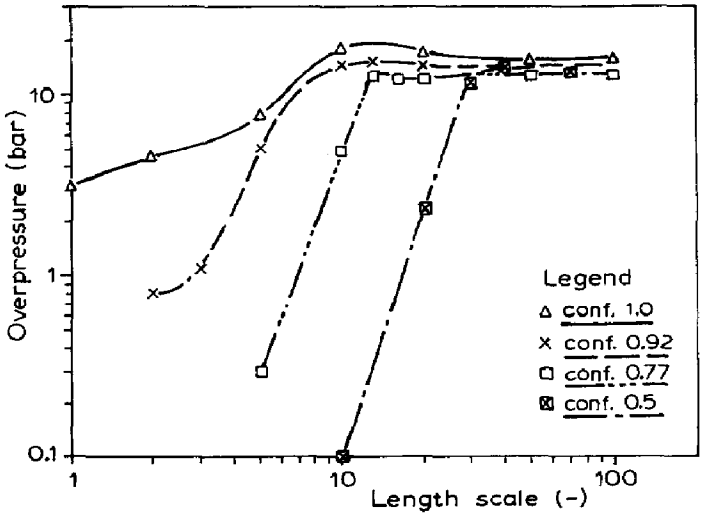

Fig. 17. Maximum overpressure vs. length scale. Obstacles along central axis of channel (Bakke and Hjertager [8]).

enclosure axis from the closed end to the open end, and ignition occurs at the closed end. The tube with a length of 10 m and diameter of 2.5 m we take as our base case and define a linear scaling factor of 1.0 for this geometry. If we, for example, increase the length of the geometry to 100 m and the diameter to 25 m,

we have for this situation, a linear scaling factor of 10. Explosion calculations have been performed over a range of scaling factors which cover three orders of magnitude, from 0.02 to 50. This corresponds to lengths of flame propagation from 20 cm to 500 m.

The channel with length of 1.22 m and height of 0.203 m (Chan et al. [29]) we take as the base and define a length scale of 1.0 for this geometry. If we for this case increase the length to 122 m and the height to 20.3 m we obtain a scaling factor of 100.

Figure 16 shows the predicted peak overpressure produced in stoichiometric mixtures of methane–air, propane–air and hydrogen–air as a function of the linear scaling factor. It can be seen that all three gases exhibit a strong dependence of peak pressure on scaling. The larger the scale, the higher the explosion pressure. Both hydrogen and propane produce larger pressures than methane. It is observed that the difference in peak pressure ratio between propane and methane in a 0.5 m tube (linear scaling equals 0.05) is 2.0, a value which is in good accordance with the experimental results reported by Hjertager [24] in a 0.5 m radial geometry.

Figure 17 shows the predicted peak overpressure produced by stoichiometric methane–air mixtures in a vented channel as function of length scale. The figure shows that the effectiveness of venting is reduced with increasing scale. For example, will a vessel of length approximately 3.6 m (scale 3) and confinement fraction on a top wall of 0.92 (8% porosity) produces a pressure of 1 bar. A scale-up of this geometry to a vessel with length of 25 m (scale 20) would produce a pressure of over 10 bars. In order to reduce the pressure to below 1 bar a confinement fraction of the top wall smaller than 50% should be chosen (porosity larger than 50%). This indicates that larger scales need larger vent areas to reduce the pressure to acceptable values.

8. Concluding remarks

A summary of a computer model capable of analysing the processes which occur in turbulent gas explosions inside complex congested geometries is presented. Several computations are reported which compare the computer model against several sets of experimental data relevant for offshore situations. The agreement between predictions and measurements is in general good. However, more work is needed: (1) to develop and verify the porosity/distributed resistance model for explosion propagation in high density obstacle fields; (2) to improve the turbulent combustion model and (3) to develop a model for deflagration to detonation transition. More experimental data are needed to enable verification of the model in high-density geometries using homogeneous as well as non-homogeneous fuel–air clouds and to validate model predictions at large and full scale. This is particularly needed for onshore process plant geometries.

Acknowledgement

The author's work on gas explosions at TMIH/TEL-TEK is financially supported by Shell Research Ltd.

References

1 B.H. Hjertager, Simulation of transient compressible turbulent reactive flows, Comb. Sci. Technol., 41 (1982) 159–170.
2 B.H. Hjertager, Numerical simulation of flame and pressure development in gas explosions, SM study No. 16, University of Waterloo Press, Waterloo, Ont., 1982, pp. 407–426.
3 B.H. Hjertager, Simulation of gas explosions, Modeling, Identification Control, 10 (1989) 227–247.
4 B.H. Hjertager, T. Solberg and K.O. Nymoen, Computer modeling of gas explosion propagation in offshore modules, J. Loss Prev. Process Ind., 5(3) (1992) 165–174.
5 B.H. Hjertager, T. Solberg and J.E. Førrisdahl, Computer simulation of the 'Piper Alpha' gas explosion accident, paper to be published, 1993.
6 J.R. Bakke and B.H. Hjertager, Quasi-laminar/turbulent combustion modelling, real cloud generation and boundary conditions in the FLACS-ICE code, CMI No. 865402-2, Chr. Michelsen Institute, 1986. Also in J.R. Bakke D. Sc. thesis, Numerical simulation of gas explosions in two-dimensional geometries, University of Bergen, Bergen, 1986.
7 J.R. Bakke and B.H. Hjertager, The effect of explosion venting in obstructed channels, In: Modeling and Simulation in Engineering, 1986, pp. 237–241.
8 J.R. Bakke and B.H. Hjertager, The effect of explosion venting in empty volumes, Int. J. Num. Meth. Eng., 24 (1987) 129–140.
9 L. Kjäldman and R. Huhtanen, Numerical simulation of vapour cloud and dust explosions, In: Numerical Simulation of Fluid Flow and Heat/Mass Transfer Processes, Vol. 18, Lecture Notes in Engineering, 1986, pp. 148–158.
10 K.D. Marx, J.H.S. Lee and J.C. Cummings, Modeling of flame acceleration in tubes with obstacles, Proc. of 11th IMACS World Congress on Simulation and Scientific Computation, Vol. 5, 1985, pp. 13–16.
11 D. Martin, Some calculations using the two-dimensional turbulent combustion code FLARE, SRD Report R373, UK Atomic Energy Authority, Warrington, 1986.
12 A.C. Van den Berg, REAGAS a code for numerical simulation of 2-D reactive gas dynamics in gas explosions, PML-TNO Report PML 1989-IN48, Rijswijk, The Netherlands, 1989.
13 B.E. Launder and D.B. Spalding, The numerical computation of turbulent flows, Computer Methods Appl. Mech. Eng., 3 (1974) 269–289.
14 B.F. Magnussen and B.H. Hjertager, On the mathematical modeling of turbulent combustion with special emphasis on soot formation and combustion, 16th Symp. (Int.) on Combustion, The Combustion Institute, Pittsburgh, PA, 1976, pp. 719–729.
15 S.V. Patankar and D.B. Spalding, A calculation procedure for heat, mass and momentum transfer in three-dimensional parabolic flows, Int. J. Heat Mass Transfer, 15 (1972) 1787–1806.
16 D.B. Spalding, A general purpose computer program for multi-dimensional one- and two-phase flow, Mathematics Computers Simulation, IMACS, XXII (1981) 267–276.
17 L.D. Cloutman, J.K. Dukowicz, J.D. Ramshaw and A.A. Amsden, CONCHAS-SPRAY: A computer code for reactive flows with fuel sprays, Los Alamos National Laboratory Report LA-9294-MS, Los Alamos, NM, May 1982.

18 J.P. Boris and D.L. Book, Flux-corrected transport I: Shasta-A fluid transport that works, J. Comp. Phys., 11 (1973) 38.
19 S.V. Patankar and D.B. Spalding, A calculation procedure for the transient and steady-state behavior of shell-and-tube heat exchangers, In: N.H. Afgan and E.V. Schlünder (eds.), Heat Exchangers: Design and Theory Sourcebook, McGraw-Hill, New York, 1974, 155–176.
20 W.T. Sha, C.I. Yang, T.T. Kao and S.M. Cho, Multi dimensional numerical modelling of heat exchangers, J. Heat Transfer, 104 (1982) 417–425.
21 W.T. Sha and B.E. Launder, A Model for Turbulent Momentum and Heat Transport in Large Rod Bundles, ANL-77-73, 1979.
22 I.O. Moen, J.H.S. Lee, B.H. Hjertager, K. Fuhre and R.K. Eckhoff, Pressure development due to turbulent flame propagation in large-scale methane–air explosions, Comb. Flame, 47 (1982) 31–52.
23 B.H. Hjertager, K. Fuhre, S.J. Parker and J.R. Bakke, Flame acceleration of propane–air in large-scale obstructed tube, 9th International Colloquium on Dynamics of Explosions and Reactive Systems, Poitiers, France, 3–8 July, 1983. See also Prog. Am. Inst. Aeronaut. Astronaut., 94 (1984) 504–522.
24 B.H. Hjertager, Influence of turbulence on gas explosions, J. Hazardous Mater., 9 (1984) 315–346.
25 J.H.S. Lee, R. Knystautas and A. Freiman, High speed turbulent deflagrations and transition to detonation in H_2–air mixtures, Comb. Flame, 56 (1984) 227–239.
26 A. Burcat, R.W. Crossley and K. Scheller, Shock tube investigation of ignition in ethane–oxygen–argon mixtures, Comb. Flame, 18 (1972) 115–123.
27 G.L. Schott and J.L. Kinsey, Kinetic studies of hydroxyl radicals in shock waves. II. Induction times in the hydrogen–oxygen reaction, J. Chem. Phys. 29 (1958) 1177–1182.
28 D.C. Bull, Concentration limits to the initiation of unconfined detonation in fuel–air mixtures, Trans. I. Chem. E., 57 (1979) 219–227.
29 C. Chan, I.O. Moen and J.H.S. Lee, Influence of confinement on flame acceleration due to repeated obstacles, Comb. Flame, 49 (1983) 27.
30 I.O. Moen, A. Sulmistras, B.H. Hjertager and J.R. Bakke, Turbulent flame propagation and transition to detonation in large fuel–air clouds, Presented at the 21st Int. Symp. on Combustion, Munich, Germany, August 3–8, 1986.
31 G.B. Kistiakowsky and L.W. Richards, Emission of vacuum ultraviolet radiation from the acetylene–oxygen and the methane–oxygen reactions in shock waves, J. Chem. Phys., 36 (1962) 1707.
32 M. Frenklach, J.H.S. Lee, J.N. White and W.C. Gardiner, Oxidation of hydrogen sulphide, Comb. Flame, 41 (1981) 1–16.
33 D.M. Solberg, Gas explosion research related to safety of ships and offshore platforms, Fuel–Air Explosions, SM Study No. 16, University of Waterloo Press, Waterloo, Ont., 1982, pp. 787–819.
34 B.H. Hjertager, K. Fuhre and M. Bjørkhaug, Gas explosion experiments in 1: 33 and 1: 5 scale offshore separator and compressor modules using stoichiometric homogeneous fuel/air clouds, J. Loss Prev. Process Ind., 1 (1988) 197–205.
35 J.R. Petrie, Piper alpha technical investigation, Interim report, Department of Energy, September 1988.
36 B.H. Hjertager, S. Enggrav, J.E. Førrisdahl and T. Solberg, A case study of gas explosions in a process plant using a 3D computer code, Paper prepared for inclusion as Appendix in Guidelines for Evaluating Consequences of Fires and Explosions from Vapor Clouds and BLEVE's, to be published by the CCPS of the AIChE, New York, 1993.